

Structural investigations and optical properties of chiral *N*-(4-nitrophenyl)-(L)-prolinol gel-grown crystals

P. Andreazza*

*Laboratoire de Minéralogie-Cristallographie, Université de Paris VI et Université de Paris VII,
Tour 16, 4 place Jussieu, 75252 Paris CEDEX, France*

D. Josse

Laboratoire de Bagneux, Centre National d'Etudes des Télécommunications, 196 rue de Paris, F-92220 Bagneux, France

F. Lefauchaux and M. C. Robert

*Laboratoire de Minéralogie-Cristallographie, Université de Paris VI et Université de Paris VII,
Tour 16, 4 place Jussieu, 75252 Paris CEDEX, France*

J. Zyss

Laboratoire de Bagneux, Centre National d'Etudes des Télécommunications, 196 rue de Paris, F-92220 Bagneux, France

(Received 1 May 1991; revised manuscript received 16 September 1991)

A gel-growth technique is used to grow highly nonlinear *N*-(4-nitrophenyl)-(L)-prolinol (NPP) single crystals of larger size with improved optical quality over those produced by other methods, such as solution or melt growth. High-quality samples are obtained by lowering the temperature of a NPP saturated water-acetonitrile mixture in a tetramethoxysilane gel. X-ray characterization gives evidence of the occurrence of twins, in agreement with the results of nonlinear optical experiments under phase-matched conditions. A close agreement between the effective interaction length with the actual physical thickness of the samples attests to their optical quality. The high quadratic nonlinear efficiency of NPP (25 times that of currently available 3-methyl-4-nitropyridine-1-oxide crystals) is confirmed. The low, monoclinic $P2_1$ symmetry of NPP does not fully determine the orientation of the principal dielectric framework. A further inspection of the orientation within the crystal unit cell of the chiral prolinol groups, together with an oriented-gas description of molecular and crystalline polarizabilities, complements the partial crystallographic information, allowing us to account fully for the orientation of the "symmetry"-free dielectric axes.

I. INTRODUCTION

Molecular crystals with charge-correlated and highly delocalized asymmetric π -electron states, such as nitroanilines, have attracted considerable attention over recent years because of their applications in nonlinear optics. The three main steps in the development of new organic nonlinear optical materials are as follows: the design and synthesis of a molecule having high nonlinearity, subsequent growth of crystals from these molecules in a noncentrosymmetric crystalline assembly, and linear and nonlinear optical studies of the crystalline samples. This last and crucial step aims both at elucidating the relations between structural and optical properties and at preliminary device demonstrations. It will eventually modify molecular-engineering ground rules, which may, in turn, yield additional insight into the molecular engineering of improved nonlinear optical crystals.

Different strategies¹ have been proposed to circumvent centrosymmetry, and to optimize dipolar orientations within the crystalline unit cell. These strategies rely on the hypothesis that dipole-dipole interactions play a key role in the general trend towards centrosymmetric packing observed in the majority (up to 80% according to

statistics¹) of molecular crystalline structures. A subsequent application of this idea led to the development of POM (3-methyl-4-nitropyridine-1-oxide) (Ref. 2) and NPP (*N*-(4-nitrophenyl)-(L)-prolinol).³ POM is the result of a strategy which advocates the cancellation of the ground-state dipole moment. A recent step in this direction has been the discovery of TATB (Ref. 4) (1,3,5-triamino-2,4,6-trinitrobenzene) as a quadratic nonlinear organic molecule with a strictly vanishing dipolar moment. This material is the result of a generalization of the nonlinear light-matter coupling scheme in the case of multipolar molecular structure.⁵ NPP exemplifies the opposite approach to the same problem, whereby dipole-dipole interactions are to be dominated by some other, stronger interactions, such as those caused by intermolecular hydrogenbondings, which, unlike dipole-dipole interactions, do not favor centrosymmetric packing.

The NPP crystal corresponds to an "optimized" crystalline structure for nonlinear interactions (there will be additional comments on this as we come to Figs. 4 and 5). Previous optical measurements^{6,7} have demonstrated the high nonlinearity of the NPP crystal ($d_{21} = 56.5 \pm 5$ pm V⁻¹). This value is one of the highest phase-matchable coefficients known for a material transparent

over a wide wavelength range extending from 0.51 to 1.65 μm . These measurements followed growth studies of NPP crystals based on modified Bridgman-Stockbarger⁸ or solution-growth⁷ techniques. However, due to possible thermal or chemical degradation of organic material, methods such as solution or gel growth at low temperature, already used with success for POM,⁹⁻¹¹ seem more promising for NPP crystal growth.¹²

Due to gelled-medium properties,¹³ gel growth allows one to obtain nearly defect-free crystals useful in optical applications. The gel is a two-phase medium formed by a three-dimensional polymer network containing the growth solution. The gel structure consequently suppresses large-scale movements, i.e., convection currents, which can disrupt crystal perfection. In addition, the probability of nucleation is largely reduced by the presence of a condensed gel phase which, during growth, is rigid enough to support the crystal, but is still compatible with the crystal development. Crystal growth then mainly takes place in the diffusion regime.

The present paper reports on the experimental conditions used for NPP crystal growth in tetramethoxysilane (TMOS) gel. Among crystals grown by this method, the particular case of twinned crystals is studied from combined crystallographic and optical points of view. The growth defects of NPP crystals are characterized by x-ray topography (Lang method). In addition, taking into account the crystalline quality of the crystals, phase-matched second-harmonic-generation (SHG) experiments have been carried out, demonstrating the high nonlinear optical performances of gel-grown NPP crystals. A small but significant discrepancy between the actual orientation of the optical dielectric framework and the main crystallographic directions is precisely measured by second-harmonic generation at phase-matched incidence. In fact, this deviation, compatible with the monoclinic structure of NPP, is due to molecular contributions attached to the chiral prolinol group of NPP molecules (shown in Fig. 12).

II. GEL GROWTH

A. The growth gelled medium

The formation of silica gels obtained from silanes requires that water be added to the growth solution: tetramethoxysilane (TMOS) uses water in a minimal (water-to-TMOS) volume ratio of 1:4 at 20°C. Preliminary NPP-solution growth experiments have allowed one to select acetonitrile (ACN) as a solvent. Various compositions of acetonitrile-water (ACN-H₂O) mixtures (all ACN-H₂O mixtures are defined here by their percentage in volume measured at 20°C) have been selected for gel growth, taking into account solute solubility, solvent volatility, and gel-formation compatibility.

The solubility of NPP in different ACN-H₂O mixtures is reported in Fig. 1. The solubility concentration is determined by gravimetry with a temperature control of $\pm 0.1^\circ\text{C}$. The solubility curves show a maximum for the 86.7 ACN-13.3 H₂O mixture. This maximum solubility is very large compared with that of pure ACN or pure

water solubilities, and varies significantly with temperature. The composition of this mixture corresponds to an azeotropic binary system, which is thermally stable. A similar behavior is observed for other organic compounds.¹¹

The ability of the solution to allow TMOS gel formation depends highly on its acidity. Gel polymerization is obtained by mixing a few percent (3-10% in volume) of TMOS in the growth solution. First, TMOS hydrolysis occurs when the pH value is close to 1 while a rapid polymerization¹⁴ takes place at higher pH values (about 6). (In fact, pH determination in slightly ionized solutions such as ACN-H₂O mixtures is questionable; as gelation in this medium proceeds in the same pH range as for aqueous solvent, pH values can nevertheless be considered as usable parameters.) Furthermore, the gelation time is an important criterion for gel selection. It depends on several parameters such as silica content, pH, and additional reagents.¹⁵ It is considered acceptable in growth experiments when it extends over less than one week. For example, gels made from a 50 ACN-50 H₂O mixture saturated with NPP (Table I) lead to a gelation time of less than five days in the case of 10% TMOS gel. For higher NPP concentrations, it is necessary to increase the medium acidity in order to obtain TMOS polymerization in a reasonable time.

Finally a 70 ACN-30 H₂O mixture has been selected for dissolving NPP and the chosen gel is a 6.5% TMOS gel which is set in three days when small amounts of HCl are added just before introducing TMOS.

Light scattering makes it possible to measure the size of the largest cavities left free by the polymer network. It

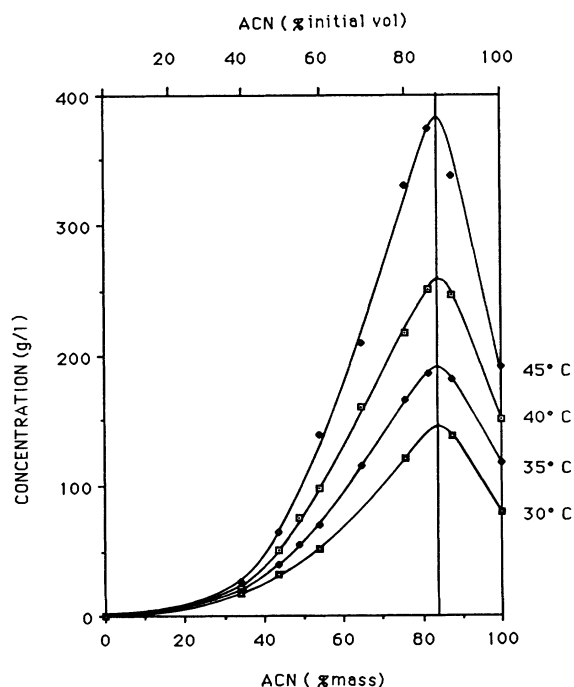


FIG. 1. Solubility curves as a function of acetonitrile percentage in the solvent for different temperatures. The maxima correspond to the azeotropic ACN-H₂O mixture.

TABLE I. The experimental growth conditions of NPP crystals are presented here. C_i , T_f , C_f are the initial and final values for temperature and concentration. T_c is the initial temperature of the controlled temperature decrease and V is the rate of the temperature decrease.

	Solvent (% vol)	TMOS (% vol)	C_{HCl} (M/l)	Temperature (°C)	C_{NPP} (g/l solvent)	V (°C/day)
Type I	50 ACN–50 H ₂ O	10	0	$T_c = 39$ $T_f = 26$	$C_i = 62$ $C_f = 26$	1.1
Type II	70 ACN–30 H ₂ O	6.5	10^{-3}	$T_c = 43$ $T_f = 23$	$C_i = 225$ $C_f = 75$	0.3

has been shown¹⁴ that for a given silica content, gel structure is only dependent on the pH of the liquid phase during polymerization. Evolution of the pH of a typical NPP growth (type II, Table I) has been consequently measured all the way through the condensation phase with a pH value ranging from 4.6 to 5.5. Blank experiments of TMOS gelation (with all reagents except NPP) have been performed for condensation pH values of 4.6 and 5.5, and measurements by light scattering lead to cavities varying from 100 to 350 Å for 7% TMOS content.

These very small values compared to pure aqueous TMOS gels¹⁴ account for the high supersaturation which is needed for nucleation¹⁶ and also for other dendritic growth phenomena, which occur quite frequently. Furthermore, the probability of twinning increases with the value of supersaturation as shown in the next sections.

B. Growth conditions

Crystals are grown by the slow cooling of a saturated gelled solution. Growth cells are immersed in a temperature-controlled water bath. Two types of experiments have been performed to obtain NPP crystals of optical quality (Table I).

In the first series of experiments (type I), a 10% TMOS gel of a 50 ACN–50 H₂O mixture saturated with NPP at 45 °C is used. The gel is subsequently formed at 50 °C, and cooled down to 39 °C in 10 min. Then, a constant cooling rate is set (see Table I) and nucleation occurs in supersaturation conditions, which are estimated from 24% to 55%, depending on experimental conditions. Higher supersaturation increases the growth rate and leads to dendritic crystals of poor optical quality. The crystals are extracted with a surrounding gel shell, and as the gel does not stick to the crystal, it can be easily pulled out with a blade without touching the crystal. Two morphologies are usually found at lower supersaturations: first, elongated rods along the a axis show small cleavage faces (101); second, (101) platelets with a thickness of about 1 mm. This morphology appears very convenient for optical characterization but only a few crystals exhibit this morphology. The solubility decrease induced by a lower temperature is nevertheless not sufficient for growing large crystals from this mixture (Fig. 2).

The second series of experiments (type II) deals with solutions of high initial NPP concentration; the limit of

solubility of NPP in a 70 ACN–30 H₂O mixture is four times larger than in a 50 ACN–50 H₂O mixture at 45 °C (Fig. 1). When HCl is added, the gel sets in three days, as the temperature is decreased. Therefore, nucleation takes place before the gel is formed with a supersaturation of about 45%. When nucleation takes place after the gel is set, the supersaturation level at nucleation cannot be measured because of gel opacity, but it is probably somewhat higher than 45%.

NPP crystals obtained in this case (type II, Table I) are larger than those obtained in type-I experiments, but their volume is less than 1 cm³. Furthermore, many crystals are twinned (about 50%). A typical habit for these crystals is shown in Fig. 3, corresponding to large (010)

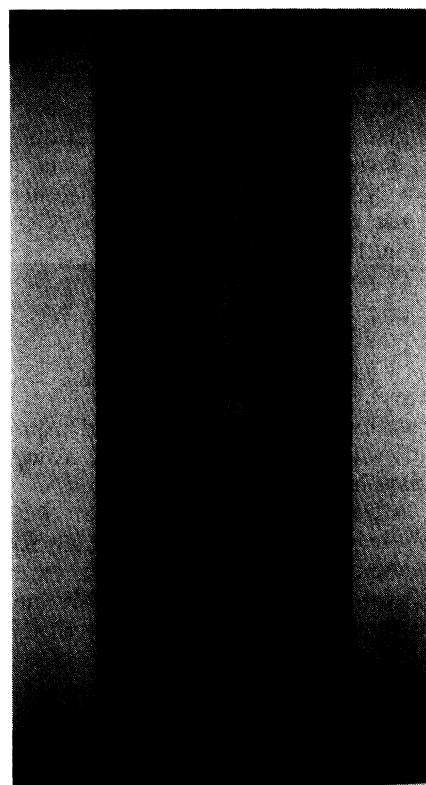


FIG. 2. Growth tube of a type-I experiment in the final growth step. The gel transparency shows NPP crystals with a thickness of a few millimeters.

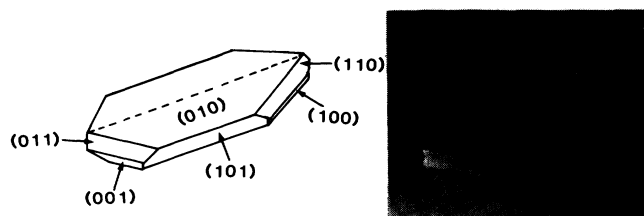


FIG. 3. NPP twinned gel-grown crystal in a type-II experiment. (a) A schematic drawing showing the different faces. (b) The crystal (the scale is millimetric).

platelets, elongated along the $[10\bar{1}]$ axis, with a twinned morphology.

III. CRYSTALLOGRAPHIC CHARACTERIZATION

A. Crystal packing and twin relations

NPP belongs to the monoclinic system with a space group $P2_1$.³ The cell parameters are $a=5.261$ Å, $b=14.908$ Å, $c=7.185$ Å, and $\beta=105.18^\circ$ with two molecules per unit cell. In a first approximation, NPP aromatic molecules can be considered as planar and lying in (101) planes. In fact, the exact position of the aromatic average plane deviates by less than 0.1° from this plane. In addition, these molecules are elongated along a direction inclined at an angle of 58.6° with respect to the binary axis. Thus, (101) planes can be considered as dense planes where molecules are linked by a hydrogen bonding network directed along the binary axis (Fig. 4).

This crystallographic arrangement is favorable to twin formation with a (101) plane as the contact plane. X-ray determination of the principal directions of each individual of a twinned crystal [Fig. 3(b)] shows that the twin axis is along $[10\bar{1}]$. The twinning can be described, according to Friedel's classification,¹⁷ as a twinning by reticular pseudomohedry with a (101) contact plane. The lattices of each individual are not in coincidence, but a multiple common pseudolattice of higher symmetry may be visualized. This lattice contains the symmetry elements of the twin and of the simple lattice, and in this case, it is pseudoorthorhombic with an obliquity of 6.5° and a multiplicity index of 3. The cells which are repeated by twin operation are drawn in Fig. 5. A small deviation ($\phi=6.5^\circ$) from an orthorhombic cell is observed; each of these cells corresponds to three elementary cells.

From an energetic point of view, twins are always the result of an accident during initial stages of crystal growth. Therefore, the following NPP twin description agrees with the requirement of minimum energy, taking into account the molecular arrangements. Let us consider the first stages of formation of one individual *B* from the other one *A*. From energetic considerations, *B* molecules of the first layer (101) occupy the same positions as *A* molecules, but they are rotated by 180° about the twin axis. This dense molecule packing is obtained by a translation of the *B* lattice by 0.5 (*a-c*) in the (101) plane

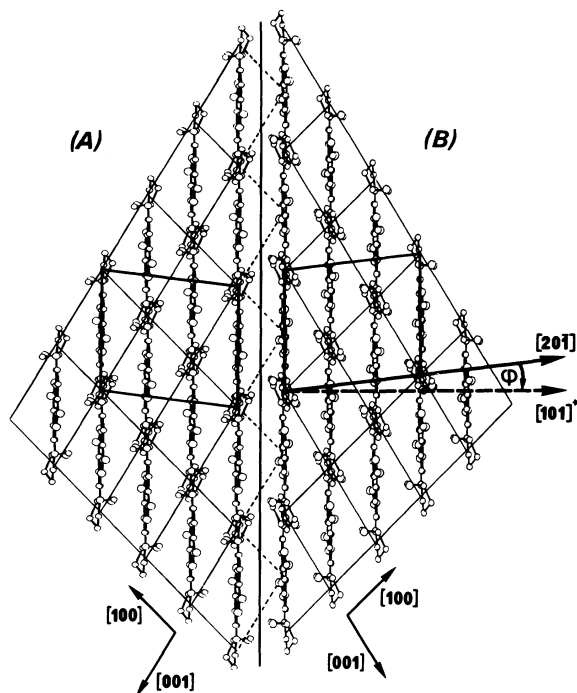


FIG. 4. NPP structure projected on the (010) plane. The central solid line marks the twin axis $[10\bar{1}]$. The dashed lines indicate the continuation of the *A* lattice into the *B* part. One unit cell of the multiple pseudocommon lattice is represented in each individual; it is oriented in the $[10\bar{1}]$ and $[20\bar{1}]$ directions.

with respect to the *A* lattice (Fig. 5).

Growth twins are usually restricted by energetic considerations to a single twinning stage at the nucleation step. In fact, very small crystals present a large free energy, which can be lowered significantly by addition of only a few molecules in either twin or normal positions. In the case of NPP gel growth, the experiments have been performed with a high initial supersaturation which favors twinning.¹⁸

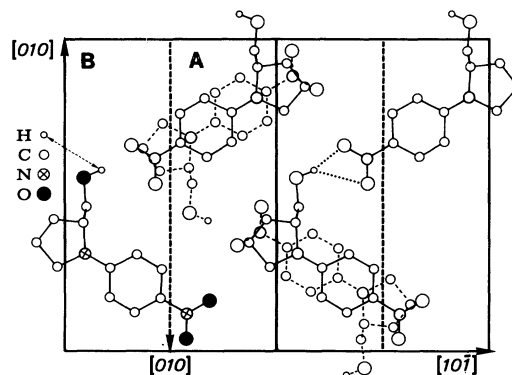


FIG. 5. Projection on the (101) contact plane of two unit cells of the *B* individual (solid lines) and of one virtual unit cell of the *A* individual (dashed lines). The dotted lines correspond to the intermolecular hydrogen bonds.

B. X-ray topographs

Type-II NPP crystals show a convenient habit (010) for x-ray topography: in fact, the molecular plane (101) which is the most efficient for diffraction (structure factor $F_h = 128$, three times larger than for the other planes) is perpendicular to the (010) platelets. Topographs are made with Cu $K\alpha$ radiation which leads to a good resolution for organic materials with a low absorption coefficient ($\mu_{\text{Cu}} = 0.76 \text{ mm}^{-1}$).

Figure 6(b) shows a translation topograph of a whole crystal which consists of two individuals *A* and *B* as discussed previously (Fig. 4). The (101) plane which is common to both individuals makes it possible to obtain a unique image. The half height width measured from this topograph is rather large ($200''$ of arc), which leads to a diffuse contrast due to lattice planes that are slightly but continuously misoriented by a total angle of less than $200''$. The two individuals can be imaged separately by diffraction from the reflecting (101) planes of each individual. These planes are symmetrical with respect to the twin axis [Figs. 6(a) and 6(c)].

The same features are visible in the topographs: a central part *D* elongated with light striations parallel to the $[10\bar{1}]$ direction and strong lines *G* parallel to the $[001]$ direction of each individual. Section topographs obtained with the $(10\bar{1})$ reflection demonstrate that these strong contrast lines *G* are located essentially at the surface of the sample and correspond to successive (110) growth horizons. One can assume that two growth steps have sequentially taken place: the former, which takes

place after nucleation at high supersaturation, develops dendrites along $[10\bar{1}]$; the latter corresponds to a slower diffusive mass transfer which allows the growth of (110) planes. Moreover, NPP crystals have been grown in solution by keeping a high supersaturation level during growth.¹² They all show a dendritic morphology with development of a serrated contour formed by (101) and (011) planes which seem to be the slowest ones at high supersaturation (45%). At a lower supersaturation rate (2% per day), the growth rate along $[100]$ becomes high so that the (110) planes are slow and the (101) planes do not grow at all [Fig. 6(d)]. It should be underlined that the dendritic part (*D*) belongs to each individual, demonstrating that twinning occurred during the first growth step at high supersaturation.

IV. LINEAR AND NONLINEAR CHARACTERIZATION

A. Optical properties

For the sake of simplicity, a convenient orthogonal reference frame (*XYZ*) linked to the crystallographic frame is conventionally chosen in order to describe the optical properties of a given crystal. However, for the low-symmetry point group 2, the *Y* axis only will coincide with the crystallographic binary axis $[010]$, while the two other dielectric axes, which lie in the (010) plane, are free, in general, to rotate about the $[010]$ axis as the light frequency is changed. Only specific molecular packing features, such as those of NPP, can lock the position of

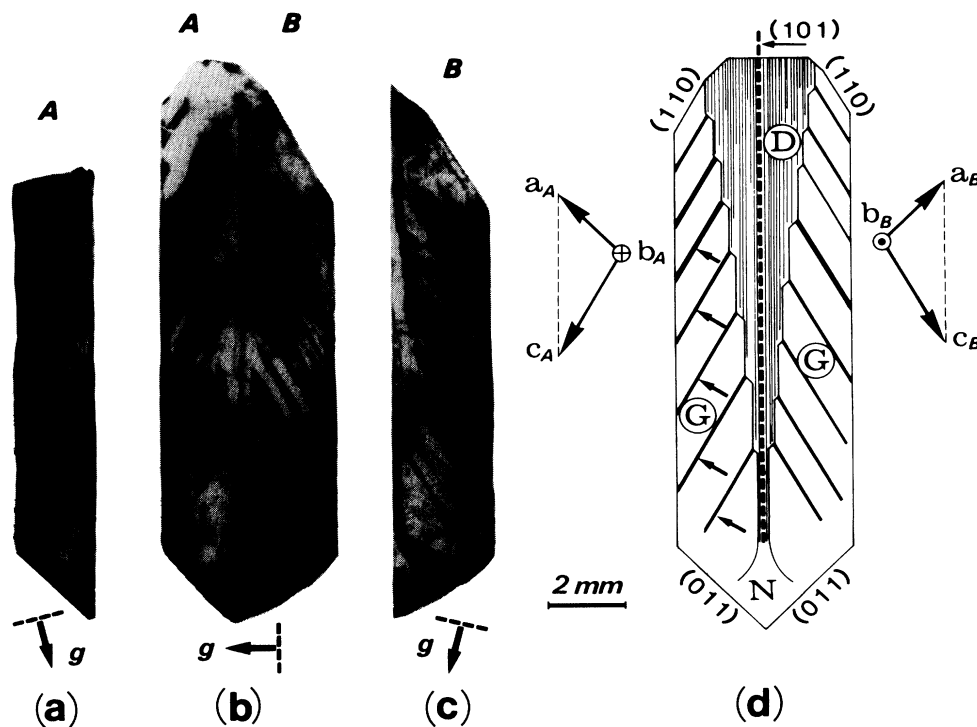


FIG. 6. Traverse x-ray topographs of a NPP twinned crystal. (a) $(10\bar{1})$ reflection, Cu $K\alpha$, *A* individual. (b) (101) reflection, Cu $K\alpha$, both individuals. (c) $(10\bar{1})$ reflection, Cu $K\alpha$, *B* individual. (d) A schematic drawing with the typical defects that have been observed (see details in the text).

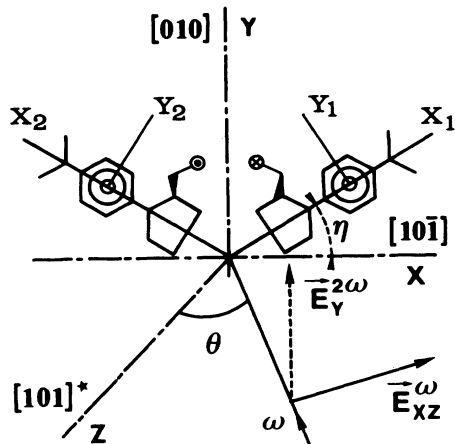


FIG. 7. Orientation of the reference frame (XYZ) with respect to the crystallographic directions. A general phase-matching configuration is indicated with the fundamental and harmonic waves polarization; $x_1y_1z_1$ and $x_2y_2z_2$ are molecular frameworks corresponding to the two molecules in the unit cell. Crystalline translations have been removed for the sake of simplicity. See also Fig. 12.

the dielectric frame, which will then become frequency independent.¹⁹ According to the particular lamellar packing of the NPP molecules in the (101) plane, and neglecting, in first approximation, the minor contribution of the out-of-plane bonds to the dielectric tensor, one may conveniently take the X axis along the $[10\bar{1}]$ direction (Fig. 7).

All the crystals presented here exhibit more or less developed (101) faces. From an experimental point of view, this morphology is very favorable for second-harmonic generation in the most efficient type-I phase-matching configuration of NPP. Indeed, according to previous calculations,⁷ phase-matched propagation directions in the near infrared are accessible from the (101) face (Fig. 7).

The phase-matching properties of NPP present a θ noncritical configuration ($d\lambda/d\theta=0$) at $\lambda=1.16\ \mu\text{m}$, for a propagation direction parallel to the Z axis. When the deviates from the Z axis in the ZX plane and the wavelength is consistently increased, the angular acceptance becomes more critical while, on the contrary, the spectral acceptance ($d\lambda/d\theta$) increases.²⁰ Considering the large transmittance at fundamental and harmonic wavelengths, experiments have been performed in this configuration with $\lambda=1.34\ \mu\text{m}$. For the fundamental wavelength, the internal incidence angle corresponding to the phase-matching is $\theta'_p=18.07^\circ$.

Two types of crystals have been studied here: (101) platelets and (010) twinned platelets. In both cases, the input and output faces for the laser beam are (101) faces.

B. Phase-matching characterization

The shape of the phase-matching rocking curve at a fixed wavelength is generally used as a quality criterion of a sample. Coupled phase-matching SHG and x-ray topography experiments allow us to relate nonlinear optical performance to crystalline quality. Earlier studies¹¹ had

shown in the case of POM that, except for macroscopic visible defects such as inclusions, only crystallographic misorientations have an adverse effect on the efficiency of second-harmonic generation. Phase-matching experiments have been performed in NPP crystals along similar lines.

The source used in this study is a CNET-made Q -switched $\text{Nd}^{3+}:\text{YAG}$ (yttrium aluminum garnet) laser emitting at $1.34\ \mu\text{m}$. The Q switch is an electro-optic LiNbO_3 cell. The energy of the emerging pulses is less than 5 mJ and their duration 80 ns in the Q -switched regime at a repetition rate of 10 Hz. The sample holder can be rotated by a stepping motor. The laser beam is horizontally polarized, i.e., normal to the rotation axis of the crystal. The harmonic beam emerging from the sample is detected after filtering, by a photodiode, and subsequently displayed.

Phase-matched SHG is obtained by rotating the sample around the twofold $[010]$ axis of the crystal, with the fundamental beam polarized perpendicularly to this axis (Fig. 7), or with the harmonic beam polarized parallel to the same axis. The phase-matching rocking curve is plotted and the effective interaction length l_{eff} can be deduced from the half-height width δ .^{2,10}

The crystal discussed here is a (101) platelet with a thickness of $0.87\ \mu\text{m}$. The angular dependence of the second-harmonic intensity is shown in Fig. 8. The calculated effective interaction length is found to be 0.67 mm, i.e., 80% of the thickness. This reduction is probably due to weak misorientations detected by x-ray topography. In spite of that, these results correspond to the best values obtained so far.

A comparison of the second-harmonic efficiencies of NPP and POM phase-matched crystals has been subsequently carried out under the same experimental conditions. The maximum second-harmonic intensity emitted by the NPP crystal is compared to that emitted by a 4.5-mm-thick POM crystal in the phase-matching configuration at $\lambda=1.34\ \mu\text{m}$.^{10,11} In order to eliminate laser fluctuations, the recorded intensity is divided by that obtained with a powder of NPP, in both cases.

Therefore, the ratio of harmonic intensities from NPP to POM corresponds to

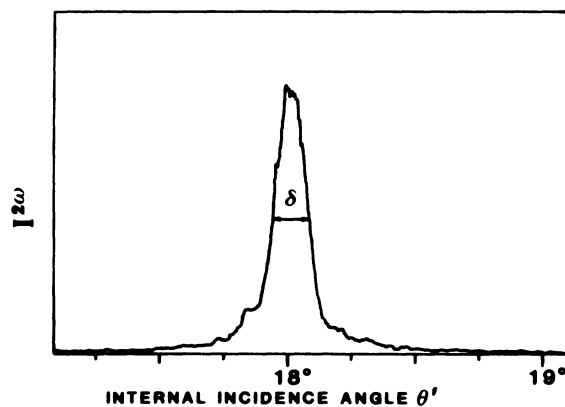


FIG. 8. Phase-matched second-harmonic intensity as a function of internal incidence angle for $\lambda=1.34\ \mu\text{m}$ (fundamental wavelength).

$$\frac{I_{\text{NPP}}^{2\omega}}{I_{\text{POM}}^{2\omega}} = 0.68, \quad (1)$$

with

$$l_{\text{eff POM}} = 3.69 \text{ mm},$$

$$l_{\text{eff NPP}} = 0.67 \text{ mm}.$$

These values allow us to deduce the SHG efficiency ratio R between NPP and POM crystals at $\lambda = 1.34 \mu\text{m}$, where the effective interaction lengths are introduced to normalize the emitted harmonic intensity,

$$R = \left(\frac{I_{\text{NPP}}^{2\omega}}{I_{\text{POM}}^{2\omega}} \right)^{1/2} \frac{l_{\text{eff POM}}}{l_{\text{eff NPP}}} = 4.55 \pm 0.1. \quad (2)$$

Thus, 1 mm of NPP is equivalent to 4.55 mm of POM, for phase-matched SHG at $\lambda = 1.34 \mu\text{m}$. In addition, from these results we can deduce the value of the highest second-order coefficient d_{21} of NPP, the only one non-negligible coefficient in the phase-matching configuration that has been used.³

In the case of type-I phase-matching SHG configuration [$n^{2\omega} = n^\omega(\theta)$], the harmonic intensity emitted by a nonlinear crystal is given by the following formula, after simplification of the original expression in Ref. 21:

$$I^{2\omega} = 2c\pi |P^{2\omega}|^2 \frac{16 \cos^4 \theta_p}{(n \cos \theta'_p + \cos \theta_p)^2} \frac{\pi^2 l_{\text{eff}}^2}{\lambda^2}, \quad (3)$$

where θ_p and θ'_p are the external and internal, respectively, incidence angles of the copropagating ω and 2ω waves with respect to the normal of the input face, and $P^{2\omega}$ is the harmonic polarization normal to the propagation plane, defined from the effective nonlinear coefficient d_{eff} (Ref. 1) by

$$P^{2\omega} = 2d_{\text{eff}} T(E^\omega)^2. \quad (4)$$

T expresses the contribution of the transmission coefficients and the sample cutting orientation with respect to the principal dielectric frame of the crystal.

With the same incoming fundamental intensity for both experiments (POM and NPP), we can deduce from Eq. (3) the value of the following expression:

$$\frac{d_{\text{eff NPP}}}{d_{\text{eff POM}}} = K \left(\frac{I_{\text{NPP}}^{2\omega}}{I_{\text{POM}}^{2\omega}} \right)^{1/2} \frac{l_{\text{eff POM}}}{l_{\text{eff NPP}}} = 1.54R. \quad (5)$$

From the effective values at $\lambda = 1.34 \mu\text{m}$ of POM (Ref. 2) ($d_{\text{eff POM}} = 7.2 \text{ pm V}^{-1}$) and NPP (Ref. 7) ($d_{\text{eff NPP}} = 0.77d_{21}$), using Eq. (5) we can obtain a value of $d_{21} = 66 \pm 5 \text{ pm V}^{-1}$ that compares satisfactorily with that determined in Ref. 7 under similar conditions. The discrepancy between the two measured values is consistent with the experimental errors.

C. Particular case of twinned crystals

Twinned crystals are of particular interest because of their increased size along the phase-matched propagation

direction: for the crystal under study, the size measured along the normal of (101) is 4.22 mm (Fig. 3).

Since the (101) plane is a symmetry plane of the index ellipsoid both individuals must simultaneously fit the phase-matching requirements for the same incidence angle. The obtained phase-matching rocking curve shows two peaks for SHG intensity (Fig. 9), which cannot be explained by a misorientation between the A and B parts of the crystal: as a matter of fact, this misorientation revealed by x-ray topography is less than $200''$ of arc.

Furthermore, due to the symmetry of the index ellipsoid, phase-matching conditions must be symmetrically fitted in the ZX plane for two propagation directions θ'_p and $-\theta'_p$ ($\theta'_p = 18.07^\circ$ at $\lambda = 1.34 \mu\text{m}$). However, the measurements show that the phase-matched propagation directions are not symmetrical with respect to the normal of the (101) input face, i.e., Z direction, which may be related to a deviation of the (101) plane, away from the $\tilde{X}\tilde{Y}$ dielectric plane.

The angle Ψ between the dielectric axis \tilde{X} and the crystallographic direction $[10\bar{1}]$, i.e., the X axis, is small, but still compatible with the observation of a significant deviation of the phase-matched directions corresponding to the two individuals of the crystal, away from the symmetric configuration. The two directions corresponding to the phase-matching in a nontwinned crystal, the angle Ψ being taken into account, are represented in Fig. 10. In the case of a twinned crystal, phase-matched SHG is obtained in four directions: $1B, 2B$ for the first individual B and $1A, 2A$ for the second individual A . Figure 11 displays schematically the different optical directions in the (010) plane.

Measurements of the external phase-matched incidence angles allow for the determination of a Ψ angle value of 0.4° with a precision of 2×10^{-2} . The crystallographic frame (XYZ) and the dielectric frame ($\tilde{X}\tilde{Y}\tilde{Z}$) are then defined according to Fig. 11 for each individual.

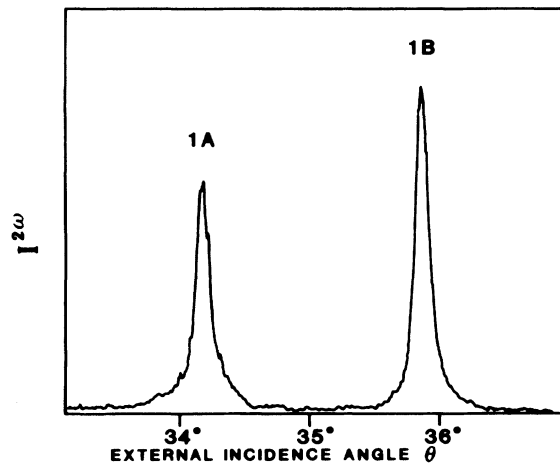


FIG. 9. Phase-matching rocking curve for a twinned crystal; the two maxima of SHG intensity correspond to phase-matching of each individual.

cules, which obviously happens for naturally defined molecular frameworks, the α polarizability tensor is identical for all N molecules and one may ignore the S labels in Eq. (7). In the case of NPP, $N=2$ and the equivalent molecular frameworks defined according to these considerations are $x_1y_1z_1$ and $x_2y_2z_2$ as represented in Figs. 7 and 12. Equation (7) represents a mere sum of N tensorial rotation terms whereby the N molecular frameworks are rotated to coincide with the crystalline axes. The principal dielectric axes are then naturally defined as the set of eigendirections of the crystalline polarizability tensor $[a]$ when it is assumed that local-field corrections will not introduce further rotations. A general derivation procedure and some physical relations derived therefrom are to be found in Ref. 22. In the case of NPP, rotation of the full tensor α by an angle η around Z yields an expression of α in the crystalline tensor XYZ , in terms of its coefficients, called $\mathcal{R}^1 \cdot \alpha$ ($\mathcal{R}^2 \cdot \alpha$) in the $x_1y_1z_1$ ($x_2y_2z_2$) molecular framework. According to a previous remark, it is not necessary to specify the 1 or 2 labels in the α matrix:

$$\mathcal{R}^{(-\varepsilon+3)/2} \alpha = \begin{pmatrix} \mathcal{R}_{xx} & \mathcal{R}_{xy} & \mathcal{R}_{xz} \\ \mathcal{R}_{xy} & \mathcal{R}_{yy} & \mathcal{R}_{yz} \\ \mathcal{R}_{xz} & \mathcal{R}_{yz} & \mathcal{R}_{zz} \end{pmatrix},$$

$$\begin{aligned} \mathcal{R}_{xx} &= \alpha_{xx} \cos^2 \eta + \alpha_{yy} \sin^2 \eta + \alpha_{xy} \sin 2\eta, \\ \mathcal{R}_{yy} &= \alpha_{xx} \sin^2 \eta + \alpha_{yy} \cos^2 \eta - \alpha_{xy} \sin 2\eta, \\ \mathcal{R}_{zz} &= \alpha_{zz}, \\ \mathcal{R}_{xy} &= \varepsilon [\alpha_{xy} \cos 2\eta + \sin 2\eta (\alpha_{yy} - \alpha_{xx}) / 2], \\ \mathcal{R}_{xz} &= \alpha_{xz} \cos \eta + \varepsilon \alpha_{yz} \sin \eta, \\ \mathcal{R}_{yz} &= \varepsilon (\alpha_{yz} \cos \eta - \alpha_{xy} \sin \eta), \end{aligned} \quad (8)$$

with $\varepsilon = \pm 1$. According to Eq. (7), the crystalline polarizability tensor $[a]$ is the average of the two rotated molecular polarizability tensors, namely,

$$[a] = \frac{1}{2} (\mathcal{R}^1 \cdot \alpha + \mathcal{R}^2 \cdot \alpha),$$

$$[a] = \begin{pmatrix} a_{XX} & 0 & a_{XZ} \\ 0 & a_{YY} & 0 \\ a_{XZ} & 0 & a_{ZZ} \end{pmatrix},$$

$$\begin{aligned} a_{XX} &= \alpha_{xx} \cos^2 \eta + \alpha_{yy} \sin^2 \eta + \alpha_{xy} \sin 2\eta, \\ a_{YY} &= \alpha_{xx} \sin^2 \eta + \alpha_{yy} \cos^2 \eta - \alpha_{xy} \sin 2\eta, \\ a_{ZZ} &= \alpha_{zz}, \\ a_{XZ} &= \alpha_{xz} \cos \eta. \end{aligned} \quad (9)$$

The cancellation of the a_{YX} and a_{YZ} coefficients results from the Y twofold symmetry invariance.

The principal dielectric axes \bar{X} and \bar{Z} are then oriented along the eigenvectors of the $[a]$ tensor in the XZ plane. Diagonalization of the $[a]$ tensor can be readily performed and leads to the expression of Ψ , as defined in Figs. 7 and 12; in terms of the $[a]$ tensor coefficients in the XZ plane

$$\tan(2\Psi) = \frac{2a_{XZ}}{a_{XX} - a_{ZZ}}. \quad (10)$$

Replacing a_{XZ} by its expression in terms of the α coefficients and introducing the Clausius-Mossotti relations^{22,23} to connect a_{XX} and a_{ZZ} to the corresponding indices of refractions n_X and n_Z , leads to the following expression:

$$\tan(2\Psi) = \left[\frac{8\pi N}{3} \cos \eta \right] [\alpha_{xz}^* (f_Z^{-1} - f_X^{-1})^{-1}], \quad (11)$$

where the classical Lorenz-Lorentz local-field correction and the Clausius-Mossotti expressions are given by

$$\begin{aligned} f_I &= (n_I^2 + 2) / 3, \\ a_{II} &= \frac{3}{4\pi N} \frac{n_I^2 - 1}{n_I^2 + 2}, \quad I = X \text{ or } Z. \end{aligned} \quad (12)$$

which N^{-1} the unit-cell volume.

Equation (11) is convenient for physical discussions and comparison with experiment or theory. It has been purposely decomposed in a product of two factors. The former one is dependent on the crystalline arrangement through the density and packing geometry ($\cos \eta$). The next factor, depending on the wavelength, is highly sensitive to the variation of the molecular structure (α_{xz}^*), and birefringence, through the local-field correction anisotropy.

It is possible to single out and infer from Eq. (11) an "experimental" value of chiral part of the molecular polarizability, which could hardly be obtained otherwise. The indices of refraction have been measured elsewhere,⁵ hence

$$\alpha_{xz}^* = 0.11 \times 10^{-24} \text{ cm}^3,$$

with $n_x = 1.916$, $n_z = 1.44$ measured at $\lambda = 1.34 \mu\text{m}$, $\Psi = 0.4^\circ$, $\eta = 31.4^\circ$,

$$N = 3.678 \times 10^{-27} \text{ cm}^{-3}.$$

This value is weak with respect to the diagonal coefficients, related to the molecular plane ($\alpha_{xz} / \alpha_{xx} \approx 3 \times 10^{-3}$). In fact, this molecular coefficient is the only one nondiagonal polarizability tensor element which is accessible to this kind of experiment.

It would be worthwhile—but outside of the scope of the present study—to connect this value of α_{xz}^* to that derived from a quantum chemical computation and further investigate this model. Whatever the limitations to the validity and accuracy of this model may prove to be, we believe that we have demonstrated the chiral origin of the rotation angle Ψ from crystalline to dielectric axes, via the contribution of the out-of-plane α_{xz}^* polarizability tensor attached to the prolinol group.

V. CONCLUSION

A gel-growth method already used for growing organic materials such as protein or POM crystals has yielded NPP crystals from a mixture of ACN and water. Com-

paratively large crystals have been obtained, showing either a (101) platelike habit or twinning with a contact plane (101) and large faces (010). Twinning is enhanced in highly supersaturated solutions, which is the case when nucleation takes place in confined media such as gelled ACN water solutions.

X-ray topographs show a uniform contrast, indicating absence of large misorientations. As growth ghosts are visible, a growth model has been proposed. Furthermore, NPP crystals are of good optical quality. Second-harmonic generation experiments in the visible have qualified gel-grown NPP crystals as the most efficient samples grown so far.

Dielectric linear and nonlinear measurements have

helped to single out the chiral contribution to the molecular polarizability of NPP. An oriented gas model of the dielectric properties accounts for the orientation of the symmetry-free principal dielectric axes and establish a relationship with the molecular structure, chiral-packing geometry, and birefringence of the crystalline lattice.

ACKNOWLEDGMENTS

The Laboratoire de Minéralogie-Cristallographie is "Unité Associée du Centre National de la Recherche Scientifique No. 9." The Laboratoire de Bagnex is "Unité Associée du Centre National de la Recherche Scientifique No. 250."

*Present address: Department of Crystals and Detectors, Quartz & Silice, Route d'Etampes, 45300 Pithiviers, France.

- ¹D. S. Chemla and J. Zyss, in *Nonlinear Optical Properties of Organic Molecules and Crystals*, edited by D. S. Chemla and J. Zyss (Academic, Orlando, FL, 1987), p. 227.
- ²J. Zyss, D. S. Chemla, and J. F. Nicoud, *J. Chem. Phys.* **74**, 4800 (1981).
- ³J. Zyss, J. F. Nicoud, and M. Coquillay, *J. Chem. Phys.* **81**, 4160 (1984).
- ⁴I. Ledoux, J. Zyss, J. S. Siegel, J. Brieno, and J. M. Leka, *Chem. Phys. Lett.* **172**, 440 (1990).
- ⁵J. Zyss, *Nonlinear Opt.* **1**, 1 (1991).
- ⁶I. Ledoux, D. Josse, P. Vidakovic, and J. Zyss, *J. Opt. Eng.* **25**, 202 (1986).
- ⁷I. Ledoux, C. Lepers, J. Badan, A. Perigaud, and J. Zyss, *Opt. Commun.* **80**, 149 (1990).
- ⁸J. Badan, R. Hierle, A. Perigaud, and P. Vidakovic, in *Nonlinear Optical Properties of Organic Molecules and Crystals* (Ref. 1), p. 308.
- ⁹R. Hierle, J. Badan, and J. Zyss, *J. Cryst. Growth* **69**, 545 (1984).
- ¹⁰D. Josse, R. Hierle, I. Ledoux, and J. Zyss, *Appl. Phys. Lett.* **53**, 2251 (1988).
- ¹¹P. Andreazza, F. Lefauchaux, M. C. Robert, D. Josse, and J. Zyss, *J. Appl. Phys.* **68**, 1 (1990).
- ¹²F. Gonzalez, M. Cunisse, A. Schan, M. C. Robert, F. Lefauchaux, P. Andreazza, A. Perigaud, and J. Zyss, *Proceedings of the VIIth European Symposium on the Material Fluid Science of Microgravity*, p. 651, Oxford, UK, 1989 (ESA 1990).
- ¹³F. Lefauchaux, M. C. Robert, S. Gits, Y. Bernard, and B. Gauthier-Manuel, *Rev. Int. Hautes Temp. Refract.* **23**, 56 (1986).
- ¹⁴B. Cabane, M. Dubois, F. Lefauchaux, and M. C. Robert, *J. Non-Cryst. Solids* **119**, 121 (1990).
- ¹⁵H. Arend and J. J. Connelly, *J. Cryst. Growth* **52**, 642 (1982).
- ¹⁶P. Andreazza, F. Lefauchaux, and B. Mutafchiev, *J. Cryst. Growth* **92**, 415 (1988).
- ¹⁷G. Friedel, *Leçons de Cristallographie* (Berger-Levrault, Paris, 1926).
- ¹⁸R. Kern, *Bull. Soc. Fr. Mineral Cristallogr.* **84**, 292 (1961).
- ¹⁹J. Zyss and J. L. Oudar, *Phys. Rev. A* **26**, 2028 (1983).
- ²⁰I. Ledoux, J. Badan, J. Zyss, A. Migus, D. Hulin, J. Etchepare, G. Grillon, and A. Antonnetti, *J. Opt. Soc. Am. B* **4**, 987 (1987).
- ²¹J. Jerphagnon and S. Kurtz, *J. Appl. Phys.* **41**, 1667 (1970).
- ²²J. Zyss and G. T. Tsoucaris, in *Structure and Properties of Molecular Crystals*, edited by M. Pierrot (Elsevier, Amsterdam, 1990), p. 297.
- ²³J. L. Oudar and J. Zyss, *Phys. Rev. A* **26**, 2016 (1982).

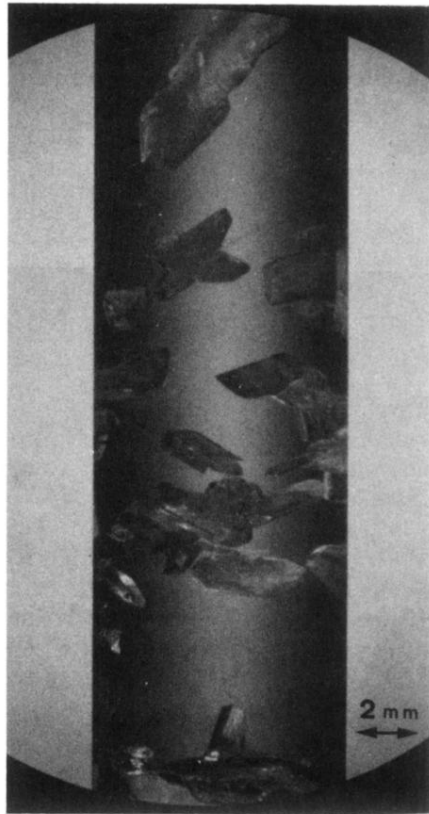


FIG. 2. Growth tube of a type-I experiment in the final growth step. The gel transparency shows NPP crystals with a thickness of a few millimeters.

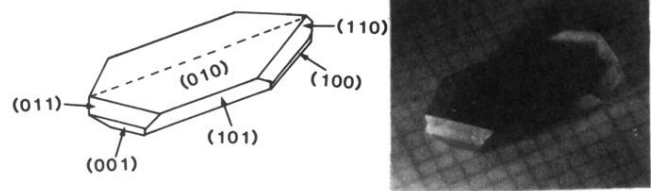


FIG. 3. NPP twinned gel-grown crystal in a type-II experiment. (a) A schematic drawing showing the different faces. (b) The crystal (the scale is millimetric).

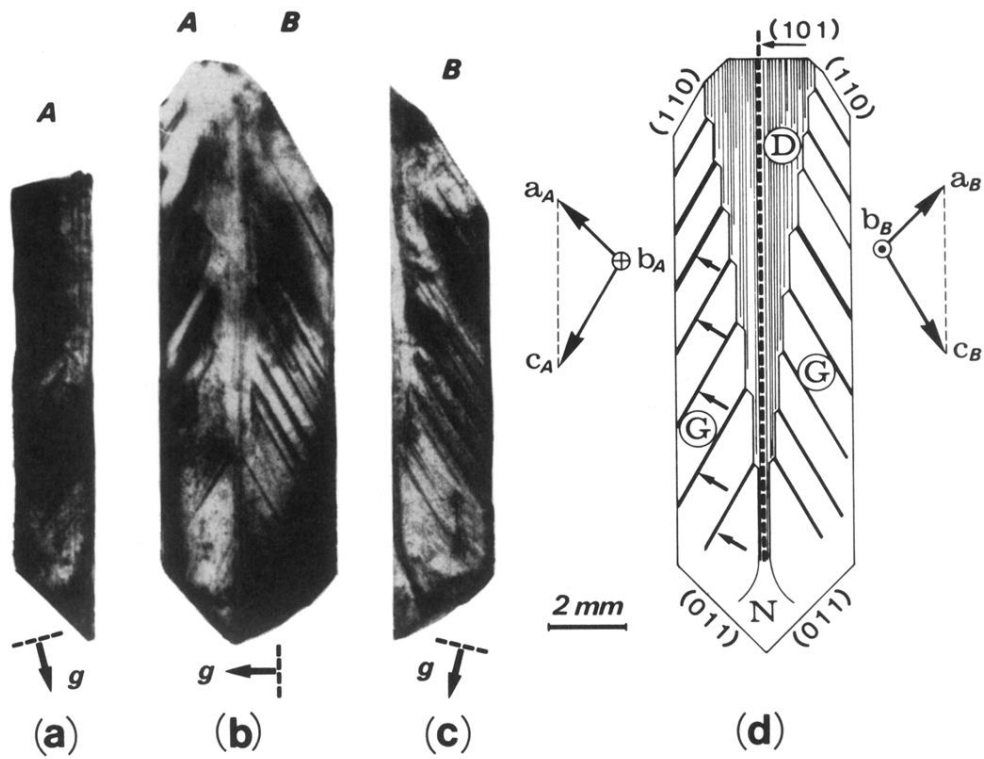


FIG. 6. Traverse x-ray topographs of a NPP twinned crystal. (a) $(10\bar{1})$ reflection, Cu $K\alpha$, *A* individual. (b) (101) reflection, Cu $K\alpha$, both individuals. (c) $(10\bar{1})$ reflection, Cu $K\alpha$, *B* individual. (d) A schematic drawing with the typical defects that have been observed (see details in the text).